ADVANCED ENERGY MATERIALS
www.advenergymat.de

High-Performance P2-Type $Na_{2/3}(Mn_{1/2}Fe_{1/4}Co_{1/4})O_2$ Cathode Material with Superior Rate Capability for Na-Ion Batteries

*Lei Liu, Xin Li, Shou-Hang Bo, Yan Wang, Hailong Chen, Nancy Twu, Di Wu, and Gerbrand Ceder**

Introduction

Because of the increasing demand from energy storage devices and the earth abundance of sodium relative to lithium, Na-ion batteries are considered as a promising alternative to the Li-ion batteries.[1–3] Over the last years, the performance of sodium transition metal layered oxides has been significantly improved,[4–12] with the energy density of some O3 or P2 type layered compounds reaching beyond 500 Wh/kg.[8,12,13] In contrast to the complicated phase transitions often observed in the O3 type layered compounds,[14,15] several P2 compounds with mixed transition metals retain the P2 phase in a wide range of Na content.[11–13,16] This is particularly important as good diffusivity of Na ions is expected in the P2 structure due to the large interslab distance and low Na diffusion barrier.[17] The best possible rate performance of a Na intercalation cathode is set by the intrinsic Na mobility in the structure. Though computational modeling has shown that this intrinsic rate capability is very good in P2-structured material,[17] the rate performance is most often degraded by Na ordering and other phase transitions. Na-vacancy ordering may trap vacancies thereby reducing the Na diffusivity, as has been observed for Li.[18,19] In addition, the flat potential associated with the two-phase region of a first-order phase transition causes an electrode to react inhomogeneously, thereby degrading the effective rate performance. In addition, phase transitions require local overpotential to nucleate followed by a strong current concentration once they are nucleated.[20] Because all these phenomena reduce the rate capability from what would be achievable based on the intrinsic Na mobility, our efforts have focused on reducing the phase transitions in P2 compounds creating large regions of solid solution.

In this communication we report a new P2 type cathode material, $Na_{2/3}(Mn_{1/2}Fe_{1/4}Co_{1/4})O_2$, showing the highest rate performance observed so far among the sodium layered cathode compounds. Consistent with our design strategy, in situ X-ray diffraction reveals a very wide single P2-phase region in $Na_x(Mn_{1/2}Fe_{1/4}Co_{1/4})O_2$ ($0.34 < x < 0.95$). Furthermore, only Na ion short range ordering instead of the long range ordering often reported in other layered compounds is observed in $Na_x(Mn_{1/2}Fe_{1/4}Co_{1/4})O_2$.[21,22] Finally, we successfully suppressed the monoclinic transition at the end of discharge that is observed in other Mn-containing P2 compounds. We believe that this judicious suppression of phase transitions is responsible for the excellent rate performance of this compound and could be repeated for other materials.

Experimental Results

P2-$Na_{2/3}(Mn_{1/2}Fe_{1/4}Co_{1/4})O_2$ (P2-MFC) was obtained via a solid-state reaction. The XRD pattern in **Figure 1** can be well refined with the hexagonal space group $P6_3/mmc$ without any diffraction peaks from impurities. The structural parameters and selected bond lengths of the P2-MFC are tabulated in Tables S1–S3, Supporting Information. As shown in Figure S1, Supporting Information, no superstructure peaks are observed in the XRD pattern, indicating no long range ordering of Na or transition metals. From the SEM image in Figure 1, the primary particles show a hexagonal layered morphology with an average size of 2–5 μm, reflecting the material's crystallographic hexagonal symmetry.

The P2-MFC material was electrochemically evaluated at different cut-off voltages and current rates. All the electrochemical tests were carried out after an initial galvanostatic discharge to

Dr. L. Liu, Prof. X. Li, Dr. S.-H. Bo, Dr. Y. Wang, Dr. N. Twu, Prof. G. Ceder
Department of Materials Science and Engineering
Massachusetts Institute of Technology
Cambridge, MA 02139, USA
E-mail: gceder@mit.edu
Prof. X. Li
John A. Paulson School of Engineering and Applied Sciences
Harvard University
Cambridge, MA 02138, USA
Prof. H. Chen
The Woodruff School of Mechanical Engineering
Georgia Institute of Technology
Atlanta, GA 30332, USA
D. Wu
Department of Mechanical Engineering
Massachusetts Institute of Technology
Cambridge, MA 02139, USA
Prof. G. Ceder
Department of Materials Sciences and Engineering
UC Berkeley
Berkeley, CA 94720, USA
Prof. G. Ceder
Materials Science Division
Lawrence Berkeley National Laboratory
Berkeley, CA 94720, USA

DOI: 10.1002/aenm.201500944

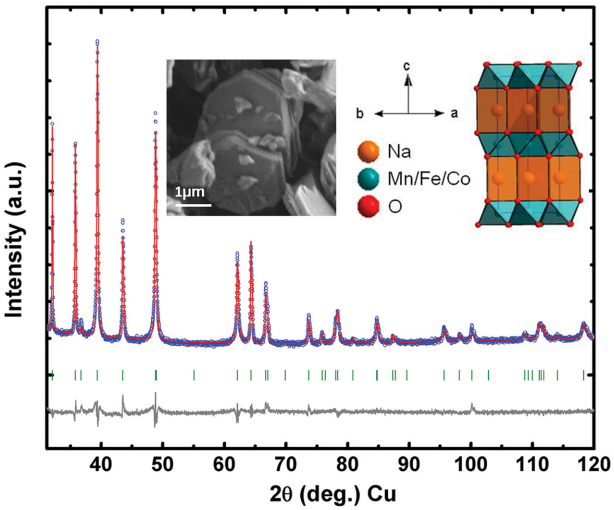

Figure 1. a) Rietveld refinement (red lines) of $Na_{2/3}(Mn_{1/2}Fe_{1/4}Co_{1/4})O_2$ in the space group of $P6_3/mmc$ (olive tick marks) using lab X-ray diffraction data (Cu K_α, blue symbols). The difference between calculated and observed patterns is shown in dark gray. The refined structure is shown in the inset. Inset: SEM image of as prepared $Na_{2/3}(Mn_{1/2}Fe_{1/4}Co_{1/4})O_2$ showing particles with plate-like shape and an average size of 2 μm.

1.5 V at 0.1 C with a typical curve shown in Figure S2, Supporting Information. P2-MFC shows a large initial discharge capacity of 195 mAh g^{-1} when cycled between 1.5 and 4.5 V as shown in **Figure 2**a. The high-voltage plateau above 4.25 V disappears upon cycling and can hardly be observed after ten cycles. When the cut-off voltage is lowered to 4.2 V (Figure 2b), the 4.25 V plateau is avoided and the cyclability is noticeably improved with an initial discharge capacity at 150 mAh g^{-1}. The difference in cyclability at different cut-off voltages is clearly demonstrated in Figure 2c.

The rate performance of P2-MFC was tested in two different modes, a slow charge followed by a fast discharge (SCFD) shown in Figure 2d, and a fast charge followed by a fast discharge (FCFD) shown in Figure 2e. The charge curves in SCFD mode were all obtained at a current rate of C/10. The major effect of increasing the discharge rate seems to be in the length and the height of low-voltage plateau. In FCFD mode polarization increases both on the low-voltage plateau and the 4.25 V plateau which shortens in charge as the rate increases to 10 and 30 C. Discharge curves/capacities in SCFD and FCFD modes are similarly indicating that the rate limitation may be more pronounced in charge. Discharge capacities of 128 and 130 mAh/g were obtained at 30 C rate in SCFD and FCFD mode, respectively, which are much larger than any previously reported layered oxide as is shown in Figure 2f, which compares the rate capability of this material to the performance of other layered materials.[7,11–13,23–25]

The structure evolution of P2-MFC during Na^+ intercalation/deintercalation was investigated with in situ XRD as shown in Figure S3, Supporting Information. **Figure 3** shows the evolution of the characteristic 002 peak and corresponding interslab distances during the initial charge/discharge process. During the charge process, the P2 phase is retained up to 34% Na concentration where a new phase, which we will refer to as "Z," starts to form through a two phase reaction between 34% and 25% Na. The Z-phase occurs as a single phase between 25% and 14% Na. We could not characterize the structure of the high-voltage phase (Z) since the peaks in the ex situ XRD pattern obtained at 4.5 V are highly broadened as shown in Figure S4, Supporting Information, which is similar to the unidentified high-voltage Z phase found previously in P2-FM by others.[16,26] Upon discharge the Z phase transforms back to the single P2 phase, which is then present for the rest of the discharge, corresponding to ≈95% Na intercalation. No P′2 phase with monoclinic distortion was observed in P2-MFC when discharged to 1.5 V, which is distinct from P2-MF.[16,27] Figure 3c shows the electron diffraction patterns along the [002] zone axis for the three samples discharged to 1.5 V (≈94% Na), pristine (≈67% Na), and charged to 4.5 V (≈14% Na), respectively. One unique feature observed by electron diffraction is the different diffuse scattering patterns observed in the 1.5 V and pristine samples with P2 structure, which indicates the evolution of Na ion short range ordering (SRO) in the Na layer upon intercalation.

Discussion

The rate performance of P2-MFC is outstanding among layered oxide materials, in particular considering that it is achieved with an average particle size above 1 μm without any further optimization. We believe that several factors are responsible for the good rate performance of P2-MFC, consistent with our strategy of suppressing phase transitions by introducing TM disorder. Indeed, from our in situ XRD results (Figure 3), a major solid solution is observed for a large range of Na content (0.34–0.95) in the P2 phase without any phase transition or long range Na ordering which is further verified by the P2 structures in the ex situ XRD patterns in Figure S6, Supporting Information. Mixing TMs in layered materials is an effective way to perturb the ordering of the transition metal sublattice and prevent sodium ions from ordering.[7,8,28] The random field the disordered TMs exert on the Na sites creates perturbations of the Na-site energy, making ordering much more difficult. Furthermore, in the low-voltage region, no P′2 phase was observed even at Na = 0.95, which is distinct from the monoclinic distortion observed in P2-$Na_xMn_{0.5}Fe_{0.5}O_2$ (P2-MF). Both P2-MFC and P2-MF have 50% Mn content, which if all were reduced to Mn^{3+} in the fully discharged state would cause a monoclinic distortion due to the strong collective Jahn-Teller effect of Mn^{3+},[21] as observed in the P2-MF.[16,27] The absence of a monoclinic distortion at the end of discharge in P2-MFC might be related to the presence of 25% Co ions. It was observed in the P2-MC system that both Co^{3+} and Mn^{4+} can be partially reduced to lower valence states during discharge,[29] which prevented the monoclinic distortion associated with the otherwise complete reduction of Mn^{4+} to Mn^{3+}. Our EELS results of P2-MFC (Figure S5 and Table S4, Supporting Information) show that Co is reduced upon discharging to 1.5 V relative to the pristine P2-MFC where the Co valence state was designed to be 3+, while the reduction of Mn or Fe in the discharged sample is not obvious. Thus, we believe it is the fact that reduction of Co^{3+} to Co^{2+} instead of Mn^{4+} to Mn^{3+} reduction in P2-MFC that gives the material the largest single-phase region among all layered cathode materials for

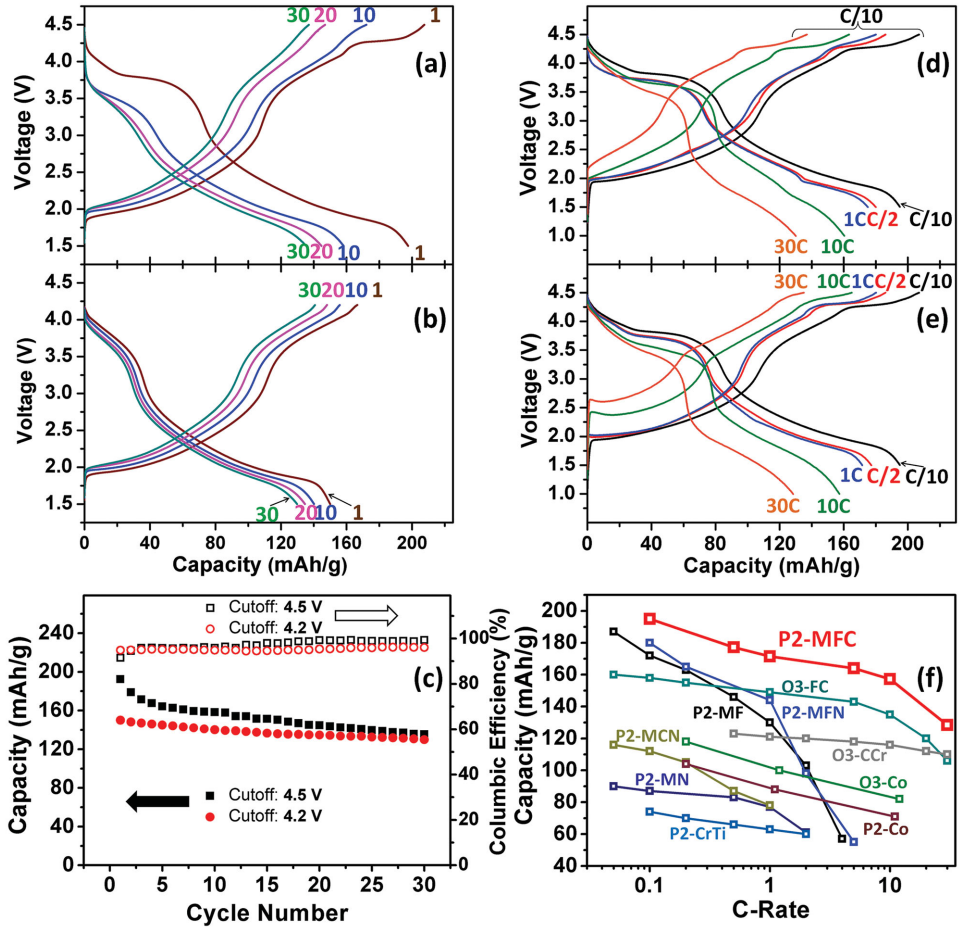

Figure 2. Electrochemical performance of $Na_{2/3}(Mn_{1/2}Fe_{1/4}Co_{1/4})O_2$. The 1st, 10th, 20th, and 30th galvanostatic charge/discharge curves at a current rate of C/10 in the voltage range of a) 1.5–4.5 V and b) 1.5–4.2 V versus Na^+/Na after initially discharging to 1.5 V. c) Cyclability of $Na_{2/3}(Mn_{1/2}Fe_{1/4}Co_{1/4})O_2$, d) and e) rate capability of $Na_{2/3}(Mn_{1/2}Fe_{1/4}Co_{1/4})O_2$ evaluated by galvanostatic charge/discharge curves in the 1st cycle were obtained in the voltage range of 1.5–4.5 V in (d) SCFD mode (slow charge and fast discharge, applying a charge current rate of C/10 and discharge current rate of C/10 to 30 C) and (e) FCFD mode (fast charge and fast discharge, applying the same charge and discharge current of C/10 to 30 C). (e) Discharge capacities of P2-$Na_{2/3}(Mn_{1/2}Fe_{1/4}Co_{1/4})O_2$ (P2-MFC) in 1st cycle in FCFD mode and discharge capacities in other reported layered materials: $NaFe_{1/2}Co_{1/2}O_2$ (O3-FC),[7] $Na_{2/3}Mn_{1/2}Fe_{1/2}O_2$ (P2-MF),[12] $Na_{0.5}(Ni_{0.23}Fe_{0.13}Mn_{0.63})O_2$ (P2-MFN),[13] Carbon-coated $NaCrO_2$ (O3-CCr),[23] $NaCoO_2$ (O3-Co),[24] $Na_{2/3}CoO_2$ (P2-Co),[24] $Na_{0.67}(Mn_{0.65}Co_{0.2}Ni_{0.15})O_2$ (P2-MCN),[11] and $Na_{2/3}Ni_{1/3}Mn_{2/3}O_2$ (P2-MN).[25] The sample loading of cathode is between 1.8 and 2.2 mg/cm^2. 1C = 258 mA g^{-1}.

Na-ion batteries. While similar electronic conductivity around $\approx 10^{-5}$ S/m was observed for several typical P2 materials as shown in Table S5, Supporting Information, the enhanced Na^+ diffusivity due to the large single phase region is a significant advantage for the rate capability of P2-MFC.

Further support for the high-rate performance of P2-MFC can also be found from recent first principle studies which suggest that P2 type materials are fast Na conductors as Na ions migrate through a honeycomb sublattice with a low intrinsic energy barrier over a wide range of Na concentration (X = 0.56–0.75).[17] As the previous work was performed on Na_xCoO_2,[17] we extended the ab initio molecular dynamics modeling to Na_xMnO_2 and Na_xFeO_2, and explored lower Na concentrations than previously studied. Details of the calculation can be found in Figure S7 and Table S5 (Supporting Information). Our results demonstrate that replacing Co with Mn or Fe does not significantly change the Na-ion diffusivity. We even find a slightly lower activation energy at low Na concentration (0.16 eV at x = 0.37) as compared to that at higher Na concentration (0.18 eV at x = 0.69). It has been found that the major limiting factor for Na migration at high Na concentration is the strong electrostatic interaction between the Na^+ ion in the activated state and the other Na^+ ions. While in an O3 structure this interaction is reduced by the operation of a divacancy mechanism,[18,19] the divacancy mechanism is not active in the P2 structure.[17] This is consistent with the increased polarization at the end of discharge in our GITT result in Figure S8, Supporting Information. It is also consistent with our rate test result (Figure 2d,e). In SCFD mode, no obvious voltage polarization was observed at the beginning of the charge curves, but the limit of the discharge capacity at high rates appears to originate from the low-voltage region at the end of discharge, indicating that this part of the capacity is more sensitive to rate. The lowered and shortened low-voltage plateau can be ascribed

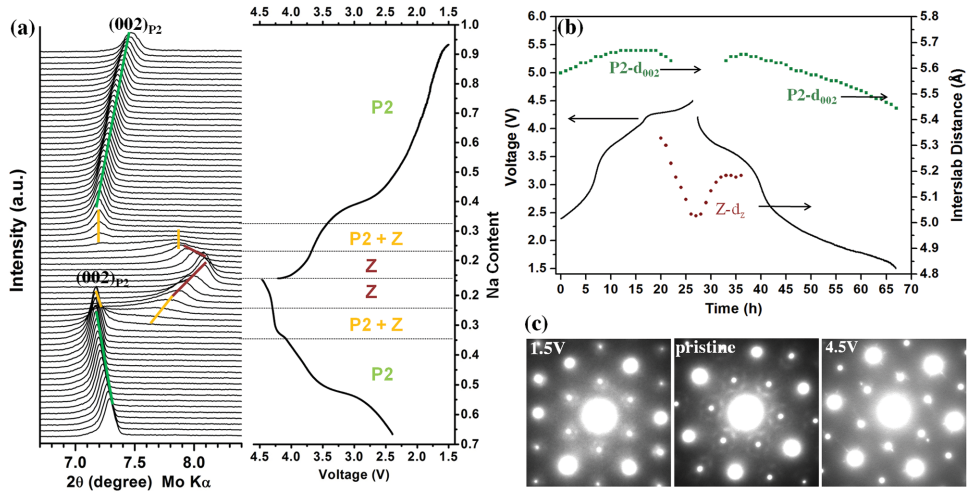

Figure 3. Structure evolution of $Na_{2/3}(Mn_{1/2}Fe_{1/4}Co_{1/4})O_2$ during the initial charge/discharge process. a) XRD patterns which were taken at 1 h scanning rate per pattern (each pattern was taken at a range of 6.5–30.5 degree, Mo Kα. Only the region around the 002 peak is shown here) and galvanostatic charge/discharge curves obtained at a current rate of C/50. b) Evolution of interslab distances in $Na_x(Mn_{1/2}Fe_{1/4}Co_{1/4})O_2$ during the electrochemical sodiation/desodiation process. c) Electron diffraction pattern of $Na_{0.95}(Mn_{1/2}Fe_{1/4}Co_{1/4})O_2$ (P2-MFC discharged to 1.5 V), $Na_{2/3}(Mn_{1/2}Fe_{1/4}Co_{1/4})O_2$, and $Na_{0.14}(Mn_{1/2}Fe_{1/4}Co_{1/4})O_2$ (P2-MFC charged to 4.5 V), which were taken along the [002] zone axis, perpendicular to the *ab* TM slab.

to increased electrochemical polarization. The diffusivity of Na^+ is slightly lower due to the lack of divacancy mechanism which will cause Na^+ concentration gradient and lower the output voltage at high rates. For the same reason, the charge curves in FCFD mode are experiencing large polarization at the beginning of charge due to low Na diffusivity, while the high-voltage parts are less dependent on rate indicating good diffusivity. The electrochemical plateau at high voltage associated with the Z phase remains present at 10 C and only partially disappears at 30 C, suggesting that the Z phase may not be a major rate limiting factor.

The cyclability of P2-MFC at high-voltage cut-off still needs to be improved as shown in Figure S9, Supporting Information. The progressive disappearance of the high-voltage plateau above 4.25 V upon cycling suggests that the P2-Z phase transition might be related to the capacity fading. Similar phenomena were also observed in some other P2 type cathode materials and O3 type layered compounds,[8,12,16,25,30] with the high-voltage phase transitions starting around 1/3 Na concentration.[8,16,27,30] Though some recent work has led to proposed theories, the nature of high-voltage phases and the mechanism connecting the phase transition and capacity fading in P2 materials are still not clear.[16,26,27]

Conclusion

P2-$Na_{2/3}(Mn_{1/2}Fe_{1/4}Co_{1/4})O_2$ was prepared and studied as a cathode materials for Na-ion batteries, in an attempt to suppress most of the first-order phase transitions occurring during desodiation. As a result, it shows so far the highest rate performance among layered oxide cathode materials. Both the wide single P2 phase region with low Na diffusion barrier and the short range ordering of Na ions may contribute to the excellent rate performance in P2-MFC. Our result suggests P2-MFC is a promising cathode candidate for application in high-power batteries.

Experimental Section

P2-$Na_{2/3}(Mn_{1/2}Fe_{1/4}Co_{1/4})O_2$ was synthesized by solid state reaction. Sodium carbonate (Na_2CO_3, Alfa, 99.95%–100.05%), Manganese oxide (Aldrich, 99%), Iron oxide (Alfa, 99.99%), Cobalt oxide (Alfa, 99.7%) were mixed in appropriate ratios and ground by high-energy ball milling. The mixture was then pressed into pellets and calcined in a box furnace. The temperature was increased at 5 °C min^{-1} to 900 °C and kept constant for 12 h. The pellets were then quenched to room temperature by throwing them on a Cu foil and transferred to an Ar-filled glovebox immediately in order to minimize air contact.

The samples were analyzed by X-ray powder diffraction on a PANalytical X'Pert pro diffractometer equipped with Cu Kα radiation. All the samples were well sealed with Kapton film to avoid air exposure during the test. Selected area electron diffraction (SAED) patterns were obtained on a JEOL 2010F transmission electron microscope. Scanning electron microscope (SEM) was obtained on a Zeiss Merlin high-resolution scanning electron microscope.

Positive electrodes consist of 80 wt% of active material, 15 wt% of carbon black, and 5 wt% of PTFE as a binder. Sodium metal was used as negative electrodes. 1 M $NaPF_6$ dissolved in a mixture of EC/DEC (1:1 v/v) was used as the electrolyte, and a glass fiber filter GF/D (Whatman) was used as the separator. Swagelok type cells were assembled in an Ar-filled glovebox and tested on a Solatron battery cycler.

The in situ cell consists of same components as the Swagelok but with a modified design to enable collection of XRD signals through a Be window. XRD patterns were continuously collected in a repeated manner on a Bruker D8 X-ray diffractometer equipped with a Mo source while the in situ cell was charged/discharged between 1.5 and 4.5 V at a rate of C/50. Each scan was carried out in the 2θ range of 6.5°–30.5° at a scan rate of 0.0067° s^{-1}.

Electronic conductivity was measured on four pellets using the four probe method. These pellets were pressed from pristine P2-MC, P2-MF, P2-MFC, and P2-MCN, respectively, and calcined at 900 °C for 2 h before the test.

Electron energy loss spectroscopy (EELS) spectra were obtained from thin specimens on a JEOL 2010F equipped with Gatan spectrometer, using parallel incident electron beam and semicollection angle of 8 mrad in TEM diffraction mode.

Supporting Information

Supporting Information is available from the Wiley Online Library or from the author.

Acknowledgements

This work was supported by the Samsung Advanced Institute of Technology.

Received: May 12, 2015
Revised: July 13, 2015
Published online:

[1] H. Pan, Y.-S. Hu, L. Chen, *Energy Environ. Sci.* **2013**, *6*, 2338.
[2] V. Palomares, P. Serras, I. Villaluenga, K. B. Hueso, J. Carretero-Gonzalez, T. Rojo, *Energy Environ. Sci.* **2012**, *5*, 5884.
[3] V. Palomares, M. Casas-Cabanas, E. Castillo-Martinez, M. H. Han, T. Rojo, *Energy Environ. Sci.* **2013**, *6*, 2312.
[4] X. Ma, H. Chen, G. Ceder, *J. Electrochem. Soc.* **2011**, *158*, A1307.
[5] P. Vassilaras, X. H. Ma, X. Li, G. Ceder, *J. Electrochem. Soc.* **2013**, *160*, A207.
[6] D. Wu, X. Li, B. Xu, N. Twu, L. Liu, G. Ceder, *Energy Environ. Sci.* **2015**, *8*, 195.
[7] H. Yoshida, N. Yabuuchi, S. Komaba, *Electrochem. Commun.* **2013**, *34*, 60.
[8] X. Li, D. Wu, Y.-N. Zhou, L. Liu, X.-Q. Yang, G. Ceder, *Electrochem. Commun.* **2014**, *49*, 51.
[9] J. Xu, D. H. Lee, R. J. Clément, X. Yu, M. Leskes, A. J. Pell, G. Pintacuda, X.-Q. Yang, C. P. Grey, Y. S. Meng, *Chem. Mater.* **2014**, *26*, 1260.
[10] D. Yuan, W. He, F. Pei, F. Wu, Y. Wu, J. Qian, Y. Cao, X. Ai, H. Yang, *J. Mater. Chem. A* **2013**, *1*, 3895.
[11] D. Buchholz, A. Moretti, R. Kloepsch, S. Nowak, V. Siozios, M. Winter, S. Passerini, *Chem. Mater.* **2013**, *25*, 142.
[12] N. Yabuuchi, M. Kajiyama, J. Iwatate, H. Nishikawa, S. Hitomi, R. Okuyama, R. Usui, Y. Yamada, S. Komaba, *Nat Mater* **2012**, *11*, 512.
[13] I. Hasa, D. Buchholz, S. Passerini, B. Scrosati, J. Hassoun, *Adv. Energy Mater.* **2014**, *4*, 1400083.
[14] S. Komaba, N. Yabuuchi, T. Nakayama, A. Ogata, T. Ishikawa, I. Nakai, *Inorg. Chem.* **2012**, *51*, 6211.
[15] M. H. Han, E. Gonzalo, M. Casas-Cabanas, T. Rojo, *J. Power Sources* **2014**, *258*, 266.
[16] B. M. de Boisse, D. Carlier, M. Guignard, L. Bourgeois, C. Delmas, *Inorg. Chem.* **2014**, *53*, 11197.
[17] Y. Mo, S. Ong, G. Ceder, *Chem. Mater.* **2014**, *26*, 5208.
[18] A. Van der Ven, G. Ceder, *Electrochem. Solid St. Lett.* **2000**, *3*, 301.
[19] A. Van der Ven, G. Ceder, *J. Power Sources* **2001**, *97–98*, 529.
[20] R. Malik, F. Zhou, G. Ceder, *Nat. Mater.* **2011**, *10*, 587.
[21] X. Li, X. H. Ma, D. Su, L. Liu, R. Chisnell, S. P. Ong, H. L. Chen, A. Toumar, J. C. Idrobo, Y. C. Lei, J. M. Bai, F. Wang, J. W. Lynn, Y. S. Lee, G. Ceder, *Nat. Mater.* **2014**, *13*, 586.
[22] R. Berthelot, D. Carlier, C. Delmas, *Nat. Mater.* **2011**, *10*, 74.
[23] C.-Y. Yu, J.-S. Park, H.-G. Jung, K.-Y. Chung, D. Aurbach, Y.-K. Sun, S.-T. Myung, *Energy Environ. Sci.* **2015**, *8*, 2019.
[24] T. Shibata, Y. Fukuzumi, W. Kobayashi, Y. Moritomo, *Sci. Rep.* **2015**, *5*, 9006.
[25] D. H. Lee, J. Xu, Y. S. Meng, *Phys. Chem. Chem. Phys.* **2013**, *15*, 3304.
[26] E. Talaie, V. Duffort, H. Smith, B. Fultz, L. Nazar, *Energy Environ. Sci.* **2015**, *8*, 2512.
[27] W. K. Pang, S. Kalluri, V. K. Peterson, N. Sharma, J. Kimpton, B. Johannessen, H. K. Liu, S. X. Dou, Z. Guo, *Chem. Mater.* **2015**, *27*, 3150.
[28] D. Carlier, J. H. Cheng, R. Berthelot, M. Guignard, M. Yoncheva, R. Stoyanova, B. J. Hwang, C. Delmas, *Dalton Trans.* **2011**, *40*, 9306.
[29] J.-H. Cheng, C.-J. Pan, J.-F. Lee, J.-M. Chen, M. Guignard, C. Delmas, D. Carlier, B.-J. Hwang, *Chem. Mater.* **2013**, *26*, 1219.
[30] Z. H. Lu, J. R. Dahn, *J. Electrochem. Soc.* **2001**, *148*, A1225.